

Underway spectrophotometry in the Fram Strait (European Arctic Ocean): a highly resolved chlorophyll *a* data source for complementing satellite ocean color

YANGYANG LIU,^{1,2,*} RÜDIGER RÖTTGERS,³ MARTA RAMÍREZ-PÉREZ,⁴
TILMAN DINTER,^{1,5} FRANÇOIS STEINMETZ,⁶ EVA-MARIA NÖTHIG,¹
SEBASTIAN HELLMANN,¹ SONJA WIEGMANN,¹ AND ASTRID BRACHER^{1,5}

¹Alfred Wegener Institute Helmholtz Centre for Polar and Marine Research, Bussesstraße 24, Bremerhaven, 27570, Germany

²Faculty of Biology and Chemistry, University of Bremen, Leobener Straße NW 2, Bremen, 28359, Germany

³Institute for Coastal Research, Helmholtz-Zentrum Geesthacht, Center for Materials and Coastal Research, Max-Planck-Straße, Geesthacht, 21502, Germany

⁴Department of Physical and Technological Oceanography, Institute of Marine Sciences, Passeig Marítim de la Barceloneta 37-49, Barcelona, 08003, Spain

⁵Institute of Environmental Physics, University of Bremen, Otto-Hahn-Allee 1, Bremen, 28359, Germany

⁶Hygeos, 165 Avenue de Bretagne, 59000 Lille, France

*yangyang.liu@awi.de

Abstract: Satellite remote sensing of chlorophyll *a* concentration (Chl-*a*) in the Arctic Ocean is spatially and temporally limited and needs to be supplemented and validated with substantial volumes of *in situ* observations. Here, we evaluated the capability of obtaining highly resolved *in situ* surface Chl-*a* using underway spectrophotometry operated during two summer cruises in 2015 and 2016 in the Fram Strait. Results showed that Chl-*a* measured using high pressure liquid chromatography (HPLC) was well related ($R^2 = 0.90$) to the collocated particulate absorption line height at 676 nm obtained from the underway spectrophotometry system. This enabled continuous surface Chl-*a* estimation along the cruise tracks. When used to validate Chl-*a* operational products as well as to assess the Chl-*a* algorithms of the aqua moderate resolution imaging spectroradiometer (MODIS-A) and Sentinel-3 Ocean Land Color Imager (OLCI) Level 2 Chl-*a* operational products, and from OLCI Level 2 products processed with Polymer atmospheric correction algorithm (version 4.1), the underway spectrophotometry based Chl-*a* data sets proved to be a much more sufficient data source by generating over one order of magnitude more match-ups than those obtained from discrete water samples. Overall, the band ratio (OCI, OC4) Chl-*a* operational products from MODIS-A and OLCI as well as OLCI C2RCC products showed acceptable results. The OLCI Polymer standard output provided the most reliable Chl-*a* estimates, and nearly as good results were obtained from the OCI algorithm with Polymer atmospheric correction method. This work confirms the great advantage of the underway spectrophotometry in enlarging *in situ* Chl-*a* data sets for the Fram Strait and improving satellite Chl-*a* validation and Chl-*a* algorithm assessment over discrete water sample analysis in the laboratory.

© 2018 Optical Society of America under the terms of the [OSA Open Access Publishing Agreement](#)

OCIS codes: (010.4450) Oceanic optics; (010.1030) Absorption.

References and links

1. T. F. Stocker, D. Qin, G.-K. Plattner, M. Tignor, S. K. Allen, J. Boschung, A. Nauels, Y. Xia, V. Bex, and P. M. Midgley, *Climate change 2013: The physical science basis: Working Group I contribution to the Fifth assessment report of the Intergovernmental Panel on Climate Change* (Cambridge University Press, 2013).

2. J. Y. Park, J. S. Kug, J. Bader, R. Rolph, and M. Kwon, "Amplified Arctic warming by phytoplankton under greenhouse warming," *Proc. Natl. Acad. Sci. U.S.A.* **112**(19), 5921–5926 (2015).
3. K. R. Arrigo and G. L. van Dijken, "Continued increases in Arctic Ocean primary production," *Prog. Oceanogr.* **136**, 60–70 (2015).
4. A. J. Kettle and M. O. Andreae, "Flux of dimethylsulfide from the oceans: a comparison of updated data sets and flux models," *J. Geophys. Res.* **105**(D22), 26793–26808 (2000).
5. M. Levasseur, "Impact of Arctic meltdown on the microbial cycling of Sulphur," *Nat. Geosci.* **6**(9), 691–700 (2013).
6. R. Y. W. Chang, S. J. Sjostedt, J. R. Pierce, T. N. Papakyriakou, M. G. Scarratt, S. Michaud, M. Levasseur, W. R. Leaitch, and J. P. Abbatt, "Relating atmospheric and oceanic DMS levels to particle nucleation events in the Canadian Arctic," *J. Geophys. Res. Atmos.* **116**(D17), D00S03 (2011).
7. P. Tunved, J. Ström, and R. Krejci, "Arctic aerosol life cycle: linking aerosol size distributions observed between 2000 and 2010 with air mass transport and precipitation at Zeppelin station, Ny-Ålesund, Svalbard," *Atmos. Chem. Phys.* **13**(7), 3643–3660 (2013).
8. C. Roesler, J. Uitz, H. Claustre, E. Boss, X. Xing, E. Organelli, N. Briggs, A. Bricaud, C. Schmechtig, A. Poteau, F. D'Ortenzio, J. Ras, S. Drapeau, N. Haëntjens, and M. Barbieux, "Recommendations for obtaining unbiased chlorophyll estimates from in situ chlorophyll fluorometers: A global analysis of WET Labs ECO sensors," *Limnol. Oceanogr. Methods* **15**(6), 572–585 (2017).
9. X. Xing, H. Claustre, E. Boss, C. Roesler, E. Organelli, A. Poteau, M. Barbieux, and F. D'Ortenzio, "Correction of profiles of in-situ chlorophyll fluorometry for the contribution of fluorescence originating from non-algal matter," *Limnol. Oceanogr. Methods* **15**(1), 80–93 (2017).
10. Y. Huot and M. Babin, "Overview of fluorescence protocols: Theory, basic concepts, and practice," in *Chlorophyll a fluorescence in aquatic sciences: methods and applications, developments in applied phycology*, E. D. Suggett et al., ed. (Springer, 2011).
11. C. C. Trees, M. C. Kennicutt II, and J. M. Brooks, "Errors associated with the standard fluorimetric determination of chlorophylls and phaeopigments," *Mar. Chem.* **17**(1), 1–12 (1985).
12. C. C. Trees, R. R. Bidigare, and J. M. Brooks, "Distribution of chlorophylls and phaeopigments in the Northwestern Atlantic Ocean," *J. Plankton Res.* **8**(3), 447–458 (1986).
13. J. Neveux, D. Delmas, J. C. Romano, P. Algarra, L. Ignatiades, A. Herbland, P. Morand, A. Neori, D. Bonin, J. Barbe, and A. Sukenik, "Comparison of chlorophyll and phaeopigment determinations by spectrophotometric, fluorometric, spectrofluorometric and HPLC methods," *Mar. Microb. Food Webs* **4**(2), 217–238 (1990).
14. M. Babin, K. Arrigo, S. Bélanger, and M.-H. Forget, *Ocean Colour Remote Sensing in Polar Seas* (IOCCG, 2015).
15. K. M. Lewis, B. G. Mitchell, G. L. van Dijken, and K. R. Arrigo, "Regional chlorophyll a algorithms in the Arctic Ocean and their effect on satellite-derived primary production estimates," *Deep Sea Res. Part II Top. Stud. Oceanogr.* **130**, 14–27 (2016).
16. B. G. Mitchell, "Predictive bio-optical relationships for polar oceans and marginal ice zones," *J. Mar. Syst.* **3**(1–2), 91–105 (1992).
17. A. Matsuoka, Y. Huot, K. Shimada, S. Saitoh, and M. Babin, "Bio-optical characteristics of the western Arctic Ocean: implications for ocean color algorithms," *Can. J. Rem. Sens.* **33**(6), 503–518 (2007).
18. S. Ben Mustapha, S. Bélanger, and P. Larouche, "Evaluation of ocean color algorithms in the southeastern Beaufort Sea, Canadian Arctic: new parameterization using SeaWiFS, MODIS, and MERIS spectral bands," *Can. J. Rem. Sens.* **38**(5), 535–556 (2012).
19. A. Matsuoka, V. Hill, Y. Huot, M. Babin, and A. Bricaud, "Seasonal variability in the light absorption properties of western Arctic waters: parameterization of the individual components of absorption for ocean color applications," *J. Geophys. Res.* **116**(C2), C02007 (2011).
20. J. Wang and G. F. Cota, "Remote-sensing reflectance in the Beaufort and Chukchi seas: observations and models," *Appl. Opt.* **42**(15), 2754–2765 (2003).
21. M. C. Serreze, M. M. Holland, and J. Stroeve, "Perspectives on the Arctic's shrinking sea-ice cover," *Science* **315**(5818), 1533–1536 (2007).
22. E. Falck, G. Kattner, and G. Budéus, "Disappearance of Pacific water in the northwestern Fram Strait," *Geophys. Res. Lett.* **32**(14), L14619 (2005).
23. R. R. Dickson, J. Meincke, and P. Rhines, *Arctic-Subarctic Ocean Fluxes: Defining the Role of the Northern Seas in Climate* (Springer, 2008), Chap. 3.
24. A. Beszczynska-Möller, E. Fahrbach, U. Schauer, and E. Hansen, "Variability in Atlantic water temperature and transport at the entrance to the Arctic Ocean, 1997–2010," *ICES J. Mar. Sci.* **69**(5), 852–863 (2012).
25. L. H. Smedsrud, A. Sorteberg, and K. Kloster, "Recent and future changes of the Arctic sea-ice cover," *Geophys. Res. Lett.* **35**(20), L20503 (2008).
26. B. Rabe, M. Karcher, U. Schauer, J. M. Toole, R. A. Krishfield, S. Pisarev, F. Kauker, R. Gerdes, and T. Kikuchi, "An assessment of Arctic Ocean freshwater content changes from the 1990s to the 2006–2008 period," *Deep Sea Res. Part I Oceanogr. Res. Pap.* **58**(2), 173–185 (2011).
27. M. H. Halvorsen, L. H. Smedsrud, R. Zhang, and K. Kloster, "Fram Strait spring ice export and September Arctic sea ice," *Cryosphere Discuss.* **9**(4), 4205–4235 (2015).
28. E. Bauerfeind, E. M. Nöthig, A. Beszczynska, K. Fahl, L. Kaleschke, K. Kreker, M. Klages, T. Soltwedel, C. Lorenzen, and J. Wegner, "Particle sedimentation patterns in the eastern Fram Strait during 2000–2005: Results

- from the Arctic long-term observatory HAUSGARTEN,” *Deep Sea Res. Part I Oceanogr. Res. Pap.* **56**(9), 1471–1487 (2009).
29. E. M. Nöthig, A. Bracher, A. Engel, K. Metfies, B. Niehoff, I. Peeken, E. Bauerfeind, A. Cherkasheva, S. Gäbler-Schwarz, K. Hardge, E. Kiliyas, A. Kraft, Y. Mebrahtom Kidane, C. Lalande, J. Piontek, K. Thomisch, and M. Wurst, “Summertime plankton ecology in Fram Strait—a compilation of long- and short-term observations,” *Polar Res.* **34**(1), 23349 (2015).
 30. A. Kraft, E. Bauerfeind, and E. M. Nöthig, “Amphipod abundance in sediment trap samples at the long-term observatory HAUSGARTEN (Fram Strait, ~ 79° N/4° E). Variability in species community patterns,” *Mar. Biodivers.* **41**(3), 353–364 (2011).
 31. P. Wassmann, D. Slagstad, and I. Ellingsen, “Primary production and climatic variability in the European sector of the Arctic Ocean prior to 2007: preliminary results,” *Polar Biol.* **33**(12), 1641–1650 (2010).
 32. P. Wassmann, “Arctic marine ecosystems in an era of rapid climate change,” *Prog. Oceanogr.* **90**(1–4), 1–17 (2011).
 33. M. Reigstad, J. Carroll, D. Slagstad, I. Ellingsen, and P. Wassmann, “Intra-regional comparison of productivity, carbon flux and ecosystem composition within the northern Barents Sea,” *Prog. Oceanogr.* **90**(1–4), 33–46 (2011).
 34. A. Forest, P. Wassmann, D. Slagstad, E. Bauerfeind, E. M. Nöthig, and M. Klages, “Relationships between primary production and vertical particle export at the Atlantic-Arctic boundary (Fram Strait, HAUSGARTEN),” *Polar Biol.* **33**(12), 1733–1746 (2010).
 35. A. Cherkasheva, A. Bracher, C. Melsheimer, C. Köberle, R. Gerdes, E. M. Nöthig, E. Bauerfeind, and A. Boetius, “Influence of the physical environment on polar phytoplankton blooms: a case study in the Fram Strait,” *J. Mar. Syst.* **132**, 196–207 (2014).
 36. G. Dall’Olmo, T. K. Westberry, M. J. Behrenfeld, E. Boss, and W. H. Slade, “Significant contribution of large particles to optical backscattering in the open ocean,” *Biogeosciences* **6**(6), 947–967 (2009).
 37. G. Dall’Olmo, E. Boss, M. J. Behrenfeld, and T. K. Westberry, “Particulate optical scattering coefficients along an Atlantic Meridional Transect,” *Opt. Express* **20**(19), 21532–21551 (2012).
 38. T. K. Westberry, G. Dall’Olmo, E. Boss, M. J. Behrenfeld, and T. Moutin, “Coherence of particulate beam attenuation and backscattering coefficients in diverse open ocean environments,” *Opt. Express* **18**(15), 15419–15425 (2010).
 39. W. H. Slade, E. Boss, G. Dall’Olmo, M. R. Langner, J. Loftin, M. J. Behrenfeld, C. Roesler, and T. K. Westberry, “Underway and moored methods for improving accuracy in measurement of spectral particulate absorption and attenuation,” *J. Atmos. Ocean. Technol.* **27**(10), 1733–1746 (2010).
 40. E. Boss, M. Picheral, T. Leeuw, A. Chase, E. Karsenti, G. Gorsky, L. Taylor, W. Slade, J. Ras, and H. Claustre, “The characteristics of particulate absorption, scattering and attenuation coefficients in the surface ocean; Contribution of the Tara Oceans expedition,” *Methods in Oceanography* **7**, 52–62 (2013).
 41. A. Chase, E. Boss, R. Zaneveld, A. Bricaud, H. Claustre, J. Ras, G. Dall’Olmo, and T. K. Westberry, “Decomposition of in situ particulate absorption spectra,” *Methods in Oceanography* **7**, 110–124 (2013).
 42. R. J. Brewin, G. Dall’Olmo, S. Pardo, V. van Dongen-Vogels, and E. S. Boss, “Underway spectrophotometry along the Atlantic Meridional Transect reveals high performance in satellite chlorophyll retrievals,” *Remote Sens. Environ.* **183**, 82–97 (2016).
 43. A. Lindfors, K. Rasmus, and N. Strömbeck, “Point or pointless - quality of ground data,” *Int. J. Remote Sens.* **26**(2), 415–423 (2005).
 44. S. Koponen, J. Attila, J. Pulliainen, K. Kallio, T. Pyhälähti, A. Lindfors, K. Rasmus, and M. Hallikainen, “A case study of airborne and satellite remote sensing of a spring bloom event in the Gulf of Finland,” *Cont. Shelf Res.* **27**(2), 228–244 (2007).
 45. G. Dall’Olmo, E. Boss, M. J. Behrenfeld, T. K. Westberry, C. Courties, L. Prieur, M. Pujo-Pay, N. Hardman-Mountford, and T. Moutin, “Inferring phytoplankton carbon and eco-physiological rates from diel cycles of spectral particulate beam-attenuation coefficient,” *Biogeosciences* **8**(11), 3423–3439 (2011).
 46. P. J. Werdell, C. W. Proctor, E. Boss, T. Leeuw, and M. Ouhssain, “Underway sampling of marine inherent optical properties on the Tara Oceans expedition as a novel resource for ocean color satellite data product validation,” *Methods in Oceanography* **7**, 40–51 (2013).
 47. G. Dall’Olmo, R. J. W. Brewin, F. Nencioli, E. Organelli, I. Lefering, D. McKee, R. Röttgers, C. Mitchell, E. Boss, A. Bricaud, and G. Tilstone, “Determination of the absorption coefficient of chromophoric dissolved organic matter from underway spectrophotometry,” *Opt. Express* **25**(24), A1079–A1095 (2017).
 48. F. Steinmetz, P. Y. Deschamps, and D. Ramon, “Atmospheric correction in presence of sun glint: application to MERIS,” *Opt. Express* **19**(10), 9783–9800 (2011).
 49. F. Steinmetz, D. Ramon, and P.-Y. Deschamps, “Algorithm Theoretical Base Document (ATBD) v1 - Polymer atmospheric correction algorithm (Issue 2.1),” (ESA Ocean Colour Climate Change Initiative (OC-CCI) Project Deliverable 2.1, 2016), <http://www.esa-oceancolour-cci.org/?q=documents#>.
 50. J. M. Sullivan, M. S. Twardowski, J. R. V. Zaneveld, C. M. Moore, A. H. Barnard, P. L. Donaghay, and B. Rhoades, “Hyperspectral temperature and salt dependencies of absorption by water and heavy water in the 400–750 nm spectral range,” *Appl. Opt.* **45**(21), 5294–5309 (2006).
 51. J. R. V. Zaneveld, J. C. Kitchen, and C. C. Moore, “Scattering error correction of reflecting-tube absorption meters,” *Proc. SPIE* **2258**, 44–55 (1994).

52. B. B. Taylor, E. Torrecilla Ribalta, A. Bernhardt, M. H. Taylor, I. Peeken, R. Röttgers, J. Piera, and A. Bracher, "Bio-optical provinces in the eastern Atlantic Ocean and their biogeographical relevance," *Biogeosci.* **8**(12), 3609–3629 (2011).
53. R. G. Barlow, D. G. Cummings, and S. W. Gibb, "Improved resolution of mono-and divinyl chlorophylls a and b and zeaxanthin and lutein in phytoplankton extracts using reverse phase C-8 HPLC," *Mar. Ecol. Prog. Ser.* **161**, 303–307 (1997).
54. J. Aiken, Y. Pradhan, R. Barlow, S. Lavender, A. Poulton, P. Holligan, and N. Hardman-Mountford, "Phytoplankton pigments and functional types in the Atlantic Ocean: a decadal assessment, 1995–2005," *Deep Sea Res. Part II Top. Stud. Oceanogr.* **56**(15), 899–917 (2009).
55. F. Vidussi, H. Claustre, B. B. Manca, A. Luchetta, and J. C. Marty, "Phytoplankton pigment distribution in relation to upper thermocline circulation in the eastern Mediterranean Sea during winter," *J. Geophys. Res. Oceans* **106**(C9), 19939–19956 (2001).
56. J. Uitz, H. Claustre, A. Morel, and S. B. Hooker, "Vertical distribution of phytoplankton communities in open ocean: An assessment based on surface chlorophyll," *J. Geophys. Res. Oceans* **111**(C8), C08005 (2006).
57. T. Hirata, N. J. Hardman-Mountford, R. J. W. Brewin, J. Aiken, R. Barlow, K. Suzuki, T. Isada, E. Howell, T. Hashioka, M. Noguchi-Aita, and Y. Yamanaka, "Synoptic relationships between surface Chlorophyll-a and diagnostic pigments specific to phytoplankton functional types," *Biogeosciences* **8**(2), 311–327 (2011).
58. R. J. Brewin, S. Sathyendranath, T. Jackson, R. Barlow, V. Brotas, R. Airs, and T. Lamont, "Influence of light in the mixed-layer on the parameters of a three-component model of phytoplankton size class," *Remote Sens. Environ.* **168**, 437–450 (2015).
59. S. N. Losa, M. A. Soppa, T. Dinter, A. Wolanin, R. J. Brewin, A. Bricaud, J. Oelker, I. Peeken, B. Gentili, V. Rozanov, and A. Bracher, "Synergistic Exploitation of Hyper-and Multi-Spectral Precursor Sentinel Measurements to Determine Phytoplankton Functional Types (SynSenPFT)," *Front. Mater. Sci.* **4**, 1–22 (2017).
60. S. G. Simis, M. Tjeldens, H. L. Hoogveld, and H. J. Gons, "Optical changes associated with cyanobacterial bloom termination by viral lysis," *J. Plankton Res.* **27**(9), 937–949 (2005).
61. R. Röttgers and S. Gehnke, "Measurement of light absorption by aquatic particles: improvement of the quantitative filter technique by use of an integrating sphere approach," *Appl. Opt.* **51**(9), 1336–1351 (2012).
62. R. Röttgers, D. Doxaran, and C. Dupouy, "Quantitative filter technique measurements of spectral light absorption by aquatic particles using a portable integrating cavity absorption meter (QFT-ICAM)," *Opt. Express* **24**(2), A1–A20 (2016).
63. K. Barker, C. Mazeran, C. Lerebourg, M. Bouvet, D. Antoine, M. Ondrusek, and L. Zibordi, "MERMAID: The MERIS MATCHup In-situ Database," in *Proceedings of the 2nd MERIS(A) ATSR User Workshop*, H. Lacoste, L. Ouwehand, ed. (ESA Communication Production Office, 2008).
64. S. W. Bailey and P. J. Werdell, "A multi-sensor approach for the on-orbit validation of ocean color satellite data products," *Remote Sens. Environ.* **102**(1), 12–23 (2006).
65. R. J. Brewin, S. Sathyendranath, D. Müller, C. Brockmann, P. Y. Deschamps, E. Devred, R. Doerffer, N. Fomferra, B. Franz, M. Grant, S. Groom, A. Horseman, C. Hu, H. Krasemann, Z. P. Lee, S. Maritorena, F. Mélin, M. Peters, T. Platt, P. Regner, T. Smyth, F. Steinmetz, J. Swinton, J. Werdell, and G. N. White III, "The Ocean Colour Climate Change Initiative: III. A round-robin comparison on in-water bio-optical algorithms," *Remote Sens. Environ.* **162**, 271–294 (2015).
66. C. Sá, D. D'Alimonte, A. C. Brito, T. Kajiyama, C. R. Mendes, J. Vitorino, P. B. Oliveira, J. C. B. Da Silva, and V. Brotas, "Validation of standard and alternative satellite ocean-color chlorophyll products off Western Iberia," *Remote Sens. Environ.* **168**, 403–419 (2015).
67. D. M. Glover, W. J. Jenkins, and S. C. Doney, *Modeling methods for marine science* (Cambridge University Press 2011).
68. C. S. Roesler and A. H. Barnard, "Optical proxy for phytoplankton biomass in the absence of photophysiology: Rethinking the absorption line height," *Methods in Oceanography* **7**, 79–94 (2013).
69. S. C. Nardelli and M. S. Twardowski, "Assessing the link between chlorophyll concentration and absorption line height at 676 nm over a broad range of water types," *Opt. Express* **24**(22), A1374–A1389 (2016).
70. A. Bricaud, M. Babin, A. Morel, and H. Claustre, "Variability in the chlorophyll-specific absorption coefficients of natural phytoplankton: Analysis and parameterization," *J. Geophys. Res. Oceans* **100**(C7), 13321–13332 (1995).
71. A. Bricaud, A. Morel, M. Babin, K. Allali, and H. Claustre, "Variations of light absorption by suspended particles with chlorophyll a concentration in oceanic (case 1) waters: Analysis and implications for bio-optical models," *J. Geophys. Res. Oceans* **103**(C13), 31033–31044 (1998).
72. D. Müller, H. Krasemann, R. J. Brewin, C. Brockmann, P. Y. Deschamps, R. Doerffer, N. Fomferra, B. A. Franz, M. G. Grant, S. B. Groom, F. Mélin, T. Platt, P. Regner, S. Sathyendranath, F. Steinmetz, and J. Swinton, "The Ocean Colour Climate Change Initiative: I. A methodology for assessing atmospheric correction processors based on in-situ measurements," *Remote Sens. Environ.* **162**, 242–256 (2015).
73. D. Müller, H. Krasemann, R. J. Brewin, C. Brockmann, P. Y. Deschamps, R. Doerffer, N. Fomferra, B. A. Franz, M. G. Grant, S. B. Groom, F. Mélin, T. Platt, P. Regner, S. Sathyendranath, F. Steinmetz, and J. Swinton, "The Ocean Colour Climate Change Initiative: II. Spatial and temporal homogeneity of satellite data retrieval due to systematic effects in atmospheric correction processors," *Remote Sens. Environ.* **162**, 257–270 (2015).

74. A. Bracher, M. Taylor, B. Taylor, T. Dinter, R. Roettgers, and F. Steinmetz, "Using empirical orthogonal functions derived from remote sensing reflectance for the prediction of phytoplankton pigments concentrations," *Ocean Sci.* **11**(1), 139–158 (2015).
75. C. Brockmann, R. Doerffer, M. Peters, S. Kerstin, S. Embacher, and A. Ruescas, "Evolution of the C2RCC neural network for Sentinel 2 and 3 for the retrieval of ocean colour products in normal and extreme optically complex waters," in *Proceedings of Living Planet Symposium*, L. Ouwehand ed. (ESA, 2016).
76. R. Doerffer and H. Schiller, "The MERIS Case 2 water algorithm," *Int. J. Remote Sens.* **28**(3–4), 517–535 (2007).
77. G. F. Cota, J. Wang, and J. C. Comiso, "Transformation of global satellite chlorophyll retrievals with a regionally tuned algorithm," *Remote Sens. Environ.* **90**(3), 373–377 (2004).
78. Z. Lee, K. L. Carder, and R. A. Arnone, "Deriving inherent optical properties from water color: a multiband quasi-analytical algorithm for optically deep waters," *Appl. Opt.* **41**(27), 5755–5772 (2002).
79. S. Maritorena, D. A. Siegel, and A. R. Peterson, "Optimization of a semianalytical ocean color model for global-scale applications," *Appl. Opt.* **41**(15), 2705–2714 (2002).
80. M. Hieronymi, D. Müller, and R. Doerffer, "The OLCI Neural Network Swarm (ONNS): A Bio-geo-optical Algorithm for Open Ocean and Coastal Waters," *Front. Mater. Sci.* **4**, 1–18 (2017).

1. Introduction

Phytoplankton, the main primary producers at the base of marine food web, have distinctive impacts on the changes of Arctic climate system. The Arctic region is warming at rates double than the global average, coinciding with persistent sea ice decline [1]. Seasonal sea ice retreat favors phytoplankton bloom development and the extension of phytoplankton growing season, increasing annual mean phytoplankton biomass and production [2,3]. This increase, in turn, is expected to further warm the ocean surface layer by absorbing more solar radiation and triggering additional positive feedbacks, which could amplify Arctic warming by 20% [2]. Meanwhile, together with ice algae, the increasing phytoplankton stocks generate more dimethylsulphide, a trace gas that provides 80% of global biogenic atmospheric sulphur [4]. When released to the atmosphere, dimethylsulphide, via formation of sulphate aerosol, cool the Arctic atmospheric temperature by dispersing solar radiation [5–7].

Despite the climatic role of Arctic phytoplankton, ship-based *in situ* measurements of total chlorophyll *a* concentration (Chl-*a*), a universal proxy of phytoplankton biomass, are sparse in the harsh Arctic Ocean. *In situ* Chl-*a* can be measured either through *in situ* fluorometers or High-Performance Liquid Chromatography (HPLC). The former method is relatively simple and inexpensive, but can cause inaccuracies due to natural variations in the fluorescence to Chl-*a* ratio [8], the fluorescence of colored dissolved organic matter (CDOM) [9], and the non-photochemical quenching [10]. HPLC is more accurate, but requires more intensive labor, time, money and complex analysis [11–13]. In addition, HPLC Chl-*a* measurements are based on discrete water samples collected on board, therefore, greatly limited by low repeat frequency and spatial coverage.

Satellite remotely sensed Chl-*a* is one of the most appropriate data sets to study long-term phytoplanktonic variability. However, ocean color data of the Arctic Ocean suffer from poor spatio-temporal coverage and resolution because of the heavy clouds and fog, the prevailing low solar elevations in high latitudes and the presence of sea ice etc [14]. Furthermore, standard ocean color Chl-*a* algorithms may not be sufficient to account for the bio-optical heterogeneity within the Arctic Ocean [15]. In the areas subjected to freshwater inputs, terrigenous CDOM can cause an overestimation of Chl-*a* when using standard algorithms [16–18]. In addition, phytoplankton tend to increase Chl-*a* per cell to absorb more light under low light conditions. Thus, pigment packaging is enhanced and Chl-*a* specific absorption coefficient is lowered, causing underestimation of satellite retrieved Chl-*a* [16–20]. Therefore, Arctic satellite ocean color Chl-*a* data require to be validated, improved and supplemented with substantial volumes of *in situ* observations.

In 2016, the Sentinel-3 Ocean and Land Color Instrument (OLCI) was launched as the successor of the Medium Resolution Imaging Spectrometer (MERIS) (mission between 2002 and 2012). It has a full spatial resolution of approximately 300 m and a swath width of 1270 km. OLCI Level 2 ocean color products were first released in July 2017. A second OLCI

sensor is launched in April 2018, followed by six more OLCI sensors operated until the late 2030s. To date, OLCI Chl-a retrievals have not yet been evaluated in the Arctic region. There is an urgent need for validation data for the new Sentinel-3 OLCI Chl-a product as well as other products.

The Fram Strait, the deepest gateway connecting the Arctic Ocean to the North Atlantic Ocean, is one of the most climate-relevant ocean passages. Water masses exchange here along with salt and heat, including southward transportation of Arctic cold fresher water and sea ice to the Atlantic by the East Greenland Current, which accounts for nearly all of the Arctic sea ice export to the Atlantic Ocean [21], and northward inflow of Atlantic warm saltier water to the Arctic Ocean carried by the West Spitsbergen Current [22,23]. Within the context of climate change, these processes have been enhanced over the past decades. Observations in the Fram Strait revealed increased warming [24] and a larger amount of Arctic freshwater and sea ice export [25–27], which further accelerated North Atlantic freshening and promoted Arctic ice melt. The consequent effects on planktonic community patterns might be inferred from the shift of dominated phytoplankton assemblages from diatoms to other smaller nano- or picoplankton species [28,29], together with an increase of warm-adapted zooplankton in the eastern Fram Strait [30]. Model simulations revealed that primary productivity differs in zones influenced by different water masses in the Fram Strait [31–34]. Recently, a time series study of summertime Chl-a in eastern Fram Strait showed increasing Chl-a trend over 20 years using combined analysis of satellite ocean color and discrete *in situ* measurements [29,35]. However, further long-term *in situ* investigations are needed as ground truth for the validation of new satellite sensors (e.g. OLCI) and evaluation of Chl-a algorithms in order to obtain consistent time series data by integrating different satellite sensor measurements.

The shipboard underway spectrophotometry represents a promising *in situ* Chl-a observation technique. It utilizes a WET Labs AC-S hyperspectral spectrophotometer (or its former alternative, the 9-wavelength resolved AC-9) that is operated in flow-through mode to derive particulate absorption coefficients (a_p) (for simplicity, the wavelength dependency of a_p is omitted in the context) [36–47]. Those a_p data are calculated by differencing measurements from temporally adjacent 0.2- μm filtered and whole water samples. Instrument drift is removed during the subtraction, which is difficult to be accounted for when routine calibrations are not possible [39]. Via empirical relationships between a_p and Chl-a, continuous surface Chl-a data along cruise tracks can be obtained. This technique considerably facilitates the collection of *in situ* Chl-a measurements with unprecedented temporal and spatial resolution due to high sampling frequency, low power consumption, and the cost-effectiveness of the AC-S or AC-9 instrument and other components of the flow-through system. While the applicability of this technique to derive highly resolved Chl-a has been evaluated on an equatorial transect [39], in Equatorial Pacific, North Atlantic, Mediterranean Sea and Subarctic Northeast Pacific [38], and during the cruises of Tara Oceans [40,46] and the Atlantic Meridional Transect [42], it has never been used in the Fram Strait.

Here, we evaluate the capability of obtaining highly resolved surface Chl-a using the shipboard underway AC-S flow-through system in the Fram Strait. To achieve a detailed understanding on the quality of the Chl-a data sets of several satellite sensors and various algorithms, the retrieved Chl-a data from AC-S a_p measurements are used to validate (1) OLCI Level 2 Chl-a operational products, (2) OLCI Level 2 Chl-a products processed with Polymer atmospheric correction algorithm (version 4.1) [48,49], and (3) Level 2 Chl-a operational products from NASA Aqua Moderate Resolution Imaging Spectroradiometer (MODIS-A).

2. Data and methods

Data were collected during two cruises onboard *R.V. Polarstern* to the Fram Strait: the PS93.2 cruise from 20 July to 14 August in 2015 and the PS99.2 cruise from 23 June to 16 July in 2016. Both cruises followed similar tracks, ranging from approximately latitudes 72° to 80°N and longitudes 10°W to 15°E (Fig. 1).

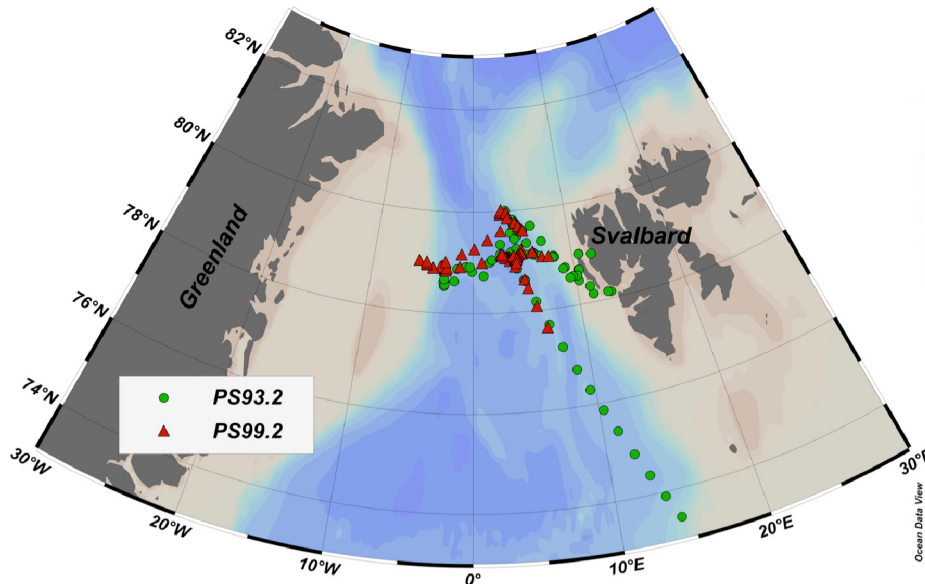


Fig. 1. Cruise tracks for PS93.2 (July-August 2015) and PS99.2 (June-July 2016) for underway HPLC data.

2.1 Underway AC-S measurements

A 25 cm-pathlength AC-S was integrated into the shipboard flow-through system to measure the hyperspectral absorption and beam attenuation coefficients over a spectral range of 400 – 740 nm. The effective spectral resolution (FWHM) is 10 nm and the sampling rate equals ~4 Hz with ~3.5 nm wavelength resolution.

The AC-S flow-through system was set up following Slade et al. [39]. The AC-S instrument was mounted to the seawater supply from the ship's membrane pump, with keel intake at roughly 11 m below the sea surface. The pumped seawater with a flow rate of 1 to 2 L min⁻¹ first passed a de-bubbler (4H Jena, Germany) to reduce air bubbles. Via an electronically actuated valve controller (Isitec, Germany), the de-bubbled seawater was diverted either directly to the AC-S to measure the total non-water absorption and beam attenuation for 50 minutes per hour, or through a 0.2- μ m cartridge filter (Sartobran P, Germany) and then to the AC-S for the remaining 10 minutes each hour to provide a baseline for particulate absorption measurements. The AC-S instrument was cleaned every 1-2 days for blank measurements. The filter cartridges were replaced approximately once per week. The system was operated constantly except when anchoring the ship in ports, during daily cleaning of the AC-S tubes or while replacing the cartridge filter.

AC-S data were processed following the procedures adapted from Slade et al. [39]. Briefly, AC-S data were successively de-spiked, visually checked and 1-min median binned. Temperature and salinity dependency of pure water absorption were accounted for following Sullivan et al. [50]. The absorption coefficients measured over the filtering period was interpolated to the time of the total absorption measurements and finally subtracted to obtain a_p and particulate attenuation coefficient (c_p). Scatter and residual temperature correction for

a_p were performed following Slade et al. [39] to correct the overestimation of a_p due to the incomplete collection of the scattered light in the AC-S a-tube, and concurrently to account for the temperature differences between the filtered and unfiltered seawater and between the samples in the AC-S tubes and the thermosalinometer. The proportional scatter correction approach from Zaneveld et al. [51] was adopted.

2.2 Discrete water sampling

To validate the AC-S measurements, approximate 5 L of water samples were collected from the unfiltered AC-S outflow for later laboratory analysis of phytoplankton pigment composition and concentration and a_p . These samples were filtered on 25 mm (or 47 mm only for a_p measurements during PS93.2) diameter Whatman GF/F glass fiber filters (nominal pore size of 0.7 μm).

2.2.1 Phytoplankton pigment analysis

Filters for phytoplankton pigment composition and concentration analysis were immediately shock-frozen in liquid nitrogen and then stored at -80°C until further analysis at the laboratories of the Alfred-Wegener-Institute Helmholtz Centre for Polar and Marine Research (AWI).

Pigment composition was analyzed by an HPLC system comprising a Waters 600 controller combined with a Waters 2998 photodiode array detector, a Waters 717plus auto-sampler and a LC Microsorb C8 HPLC column. A list of 23 pigments shown in Table 2 of Taylor et al. [52] were separated and quantified following an adjustment of the method described in Barlow et al. [53], as detailed in Taylor et al. [52]. The pigment data were quality assured according to Aiken et al. [54]. Chl-*a* was calculated as the summed contribution of monovinyl chlorophyll *a*, chlorophyllide *a* and divinyl chlorophyll *a* concentrations. Four phytoplankton groups, namely diatoms, green algae, prymnesiophytes (haptophytes) and prokaryotes, were identified and determined from their biomarker pigments using Diagnostic Pigment Analysis (DPA) [55–58] that is applied to a large global pigment data set by Losa et al. [59] to obtain the specific weights to convert the diagnostic pigment concentrations to Chl-*a* contributed by the aforementioned phytoplankton groups.

2.2.2 Particulate absorption measurements

The Quantitative Filter Technique (QFT) measurements of spectral light absorption were performed differently over the two cruises. Filters collected during PS93.2 were stored at -80°C after being immediately shocked-frozen in liquid nitrogen until analysis at AWI. Measurements were carried out on a dual-beam UV/VIS spectrophotometer (Cary 4000, Varian Inc.) equipped with a 150 mm integrating sphere (external DRA-900, Varian, Inc. and Labsphere Inc., made from Spectralon™) following the method described in Simis et al. [60]. The filters were placed in the center of the integrating sphere and scanned in the range from 300 to 850 nm with the wavelength resolution of 1 nm. The baseline was recorded using a dry blank filter and a blank filter that was soaked in freshly produced Milli-Q water for more than 30 minutes. Optical density ($OD(\lambda)$) was measured and transformed to transmittance ($T(\lambda)$) following Eq. (1), which was finally used to calculate a_p following Eq. (2) using a path length amplification factor of 4.5 ($\beta = 1/4.5$) [61].

$$T(\lambda) = e^{-OD(\lambda)} \quad (1)$$

$$a_p(\lambda) = -\ln(T(\lambda)) \times A \times \beta \times V^{-1} \quad (2)$$

where V is the filtrated sample volume in m^3 , A the filter clearance area in m^2 and λ wavelength in nm. The calculated a_p is in m^{-1} .

Filters collected during PS99.2 were immediately measured on board with QFT using a small portable integrating cavity absorption meter (QFT-ICAM) to avoid the artifacts and

uncertainties from sample preservation and transport. Instrument setup and measurement procedure were detailed in Röttgers et al. [62]. Briefly, QFT-ICAM is made up of an 80 mm-diameter integrating spherical cavity with the highly reflective white PTFE walls, a CF-1000-HC lamp (Illumination Technology, USA) with an integrated filter wheel and a photodiode array detector (AVASPEC-ULS2048-RS-USB2, Avantes, the Netherlands). These three components are connected by two quartz-glass optical fibers. There are two thin Nylon strings in the middle plane across the whole cavity to hold the filters. Sample and reference filters were measured inside the integrating cavity by being moved in and outside of the light beam. A scan from 300 nm to 850 nm with the wavelength resolution of 0.3 nm was performed for each measurement. Dark currents were determined before filter measurements. a_p was calculated following Eqs. (1) and (2) using a path length amplification of 4.06 ($\beta = 1/4.06$) [62].

2.3 Satellite Chl-a validation

In situ Chl-a data derived from both AC-S and HPLC were used to validate satellite-derived Chl-a products. MODIS-A Level 2 operational products (R2014.0) retrieved from OCI algorithm were downloaded from the Ocean Color Website (<http://oceancolor.gsfc.nasa.gov/>) and analyzed for both *in situ* data sets of PS93.2 and PS99.2.

OLCI Level 2 Chl-a products were also validated with the PS99.2 data set, since OLCI started measuring in 2016. In this case, Chl-a products retrieved from Case 2 Regional CoastColour (C2RCC, version 0.15) and OC4 standard processor algorithms were used. OLCI Level 2 products (reprocessed data set REP NT_002 IPF-OL-2, version 06.08) were provided by EUMETSAT (<https://www.eumetsat.int>) in the context of Sentinel-3 Validation Team (S3VT) project.

In addition, three Chl-a data products produced from OLCI remote sensing reflectance data using Polymer atmospheric correction algorithm (version 4.1) were also evaluated because of their increased coverage as compared to the standard products. The Polymer algorithm provides a powerful atmospheric correction for ocean color data in the presence of contamination from sun glint, thin clouds heavy aerosol plumes or adjacency effect; these contaminated conditions are often not correctly treated by standard atmospheric correction schemes with extrapolation from the near infrared (e.g., used for MODIS-A OCI and OLCI OC4) [48,49]. We processed OLCI Level 1 products (reprocessed data set REP NT_002 IPF-OL-1-EO, version 06.06) from EUMETSAT with the Polymer algorithm (version 4.1) (provided at www.hygeos.com/Polymer). We used the Chl-a product retrieved from the Polymer atmospheric correction processing, which is an iterative spectral matching method using OLCI bands from 412 to 865 nm. This method relies on two simple models: a three-parameter model for the atmosphere and a two-parameter model for the ocean. The latter is based on a backscattering and an absorption term that is represented by Chl-a. Therefore, Polymer produces not only normalized spectral water reflectance but also Chl-a estimates. In this configuration, no adjustment of the radiometric calibration has been applied: the gain is set to 1 at all bands. Additionally, we applied the OCI and OC4 algorithms to the OLCI Polymer remote sensing reflectance to derive Chl-a products, which helps to evaluate specifically the effect of atmospheric correction methods on the different OLCI and MODIS-A products. Here we denote the OC4 algorithm with standard atmospheric correction as OC4-Operational, OCI and OC4 algorithm with Polymer atmospheric correction as OCI- and OC4-Polymer, respectively, and Polymer standard algorithm as Polymer-Standard.

When processing OLCI data, different bitmask settings were applied to approve only pixels measured under optimal conditions. S3VT recommends bitmask settings for the OC4 standard product as follows: [invalid, land, cloud, cloud_ambiguous, cloud_margin, snow_ice, suspect, hisolzen, saturated, highglint, whitecaps, ac_fail, oc4me_fail, annot_tau06, rwneg_o2, rwneg_o3, rwneg_o4, rwneg_o5, rwneg_o6, rwneg_o7, rwneg_o8] and for the C2RCC product as follows: [invalid, land, cloud, cloud_ambiguous, cloud_margin, snow_ice,

suspect, hisolzen, saturated, highglint, whitecaps, ocnn_fail]. For the Polymer output, a [thick_aerosol, cloud_base] bitmask was applied.

In situ Chl-a data sets were then matched to satellite derived Chl-a values at the same day for MODIS-A 1x1 and OLCI 3x3 pixel windows following the procedure of MERMAID (MERIS Matchup In situ Database) [63]. Different pixel window sizes were chosen because of the relatively comparable spatial resolutions of 1 km for MODIS-A 1x1 and 900 m (3x300 m) for OLCI 3x3 pixel windows. Both MODIS-A and Sentinel-3 orbits are near-polar orbits. In polar regions, it is more possible to acquire multiple satellite retrievals for a given *in situ* record due to the increasing overlap in adjacent swaths. In this case, the multiple satellite data are considered as parallel measurements and included in the same pixel window. Satellite Chl-a data for which the median coefficients of variation with respect to log10 based Chl-a within one pixel window were greater than 0.15 were excluded to minimize the effect of mismatch in spatial scales of *in situ* and satellite data [64]. When more than one *in situ* measurements were matched to satellite data within the same pixel window, the *in situ* Chl-a values were averaged. Table 1 shows an overview over all the algorithms that are used to derive Chl-a products.

Table 1. Satellite Chl-a algorithms being evaluated for the cruises PS93.2 and PS99.2.

Cruises	Satellite Sensor	Atmospheric Correction	Chl-a algorithm	Denotation
PS93.2	MODIS-A	Standard	OCI	OCI
PS99.2	MODIS-A	Standard	OCI	OCI
		OLCI	OC4	OC4-Operational
		C2RCC	C2RCC	C2RCC
		Polymer	Polymer	Polymer-Standard
		Polymer	OC4	OC4-Polymer
	Polymer	OCI	OCI-Polymer	OCI-Polymer

2.4 Statistics

We used a set of statistical tests following Brewin et al. [65] and Sá et al. [66] to evaluate the performance of (1) the AC-S data correction scheme, (2) AC-S based Chl-a retrieval models and (3) satellite Chl-a algorithms. These tests include the determination coefficient (R^2), the Pearson correlation coefficient (r), the root mean square error ($RMSE$), the mean absolute error (MAE), the bias error (δ), and the unbiased root mean square error (Δ), the mean Relative Percentage Difference (RPD) and the slope (S) and the intercept (I) of Type-2 regression. For all linear regressions, Type-2 regression analysis was used (MATLAB function lsqfitma.m) [67]. The equations for these statistical metrics are given below:

$$RMSE = \sqrt{\frac{1}{N} \sum_{i=1}^N (C_i^E - C_i^M)^2} \quad (3)$$

$$MAE = \frac{1}{N} \sum_{i=1}^N |C_i^E - C_i^M| \quad (4)$$

$$\delta = \frac{1}{N} \sum_{i=1}^N (C_i^E - C_i^M) \quad (5)$$

$$\Delta = \sqrt{\frac{1}{N} \sum_{i=1}^N [(C_i^E - \mu^E) - (C_i^M - \mu^M)]^2} \quad (6)$$

$$RPD = \frac{1}{N} \sum_{i=1}^N \frac{C_i^E - C_i^M}{C_i^M} \times 100 \quad (7)$$

where N is the total number of samples, i is the sample index, C is Chl-a (log-transformed except in (7)) and μ is the averaged C . The superscript E denotes the estimated value (e.g. from satellite data) and the superscript M the measured value (e.g. from *in situ* data).

3. Results and discussion

3.1 Chl-a estimation from AC-S

In this study, particulate absorption line height at 676 nm ($a_{LH}(676)$) is used to retrieve Chl-a. $a_{LH}(676)$ is chosen because it provides good estimates of Chl-a with lower contribution of accessory pigments and weaker packaging effect [68, 69]. $a_{LH}(676)$ was calculated from the particulate absorption coefficient at 676 nm above the baseline from 650 nm to 715 nm following Eq. (8) [68]. For both cruises, $a_{LH}(676)$ derived from the AC-S and filter-pad data are linearly related (for PS93.2, $r = 0.94$, $RMSE = 0.008$; for PS99.2, $r = 0.90$, $RMSE = 0.009$).

$$a_{LH}(676) = a_p(676) - \frac{a_p(715) - a_p(650)}{715 - 650} \times (676 - 650) - a_p(650). \quad (8)$$

AC-S derived $a_{LH}(676)$ calculated from Eq. (8) was related to HPLC Chl-a data for the two cruises in order to derive Chl-a from all the AC-S data. $a_{LH}(676)$ was log10 transformed and averaged within the period of 10 minutes before and after HPLC sampling time [42]. It was then back-transformed and related to HPLC Chl-a data by the robust fitting of the power function of Eq. (9) [70,71] using bisquare weighting scheme:

$$Chl - a = A a_{LH}(676)^B. \quad (9)$$

Table 2 portrays the regression coefficients and statistics for Chl-a to $a_{LH}(676)$ relationships. $a_{LH}(676)$ and HPLC Chl-a data were both log10-transformed for the calculation of the statistical metrics. For PS93.2, the coefficients A and B are 86.1 ± 11.1 and 1.00 ± 0.03 , respectively; for PS99.2, they are 36.2 ± 6.78 and 0.93 ± 0.05 , respectively. The fits are shown in Fig. 2(a)-2(b). B value from PS93.2 is close to 1, indicating a linear relationship between Chl-a and $a_{LH}(676)$. A value from PS93.2 is over twice greater than that from PS99.2. For comparison, the relationships between Chl-a and filter-pad $a_{LH}(676)$ were also derived (Table 2). The different fits obtained from AC-S and filter-pad data could be attributed to (1) varying degrees of sample-to-sample β variations for filter-pad data, (2) sensitivity of the calculated absorption coefficient to filter clearance area (1 mm measurement error for diameter causes 0.008 m^{-1} error in absorption coefficient), and (3) a wider spectral bandwidth of AC-S (10 nm) compared to Cary and QFT-ICAM (approximately 2 nm) resulting in flattening absorption peaks with AC-S data. Filter-pad data measured by Cary and QFT-ICAM can also differ from each other because samples for QFT-ICAM were immediately measured after filtration, whereas samples for Cary were stored at -80°C before finally measured. Nevertheless, the good R^2 , $RMSE$ and MAE values support the use of AC-S flow-through system to obtain Chl-a with high quality.

Given the good HPLC Chl-a to AC-S $a_{LH}(676)$ relationships found for both cruises, coefficients A and B were then applied to all the AC-S derived $a_{LH}(676)$ data to retrieve continuous surface Chl-a data sets along the cruise tracks. Figure 3 shows the comparison between Chl-a derived from the underway AC-S flow-through system and HPLC measurements for both cruises. The two Chl-a data sets showed good consistency, with S and I being 0.97 ± 0.02 and 0.03 ± 0.02 , and the log10 based r , $RMSE$ and MAE being 0.95, 0.097 and 0.064, respectively. In total, 24424 and 16110 Chl-a data were generated for PS93.2 and PS99.2, ranging from 0.179 to 3.550 mg m^{-3} (mean value: 1.042 mg m^{-3}) and from 0.003 to

2.701 mg m^{-3} (mean value: 0.677 mg m^{-3}), respectively. These values are representative for the summertime Chl-a variability observed in the Fram Strait [34]. The histograms of both *in situ* Chl-a distribution (Fig. 2(c) and 2(d)) and time series of Chl-a (Fig. 4(a) and 4(b)) show that Chl-a data derived from AC-S exhibit a general agreement with those from HPLC, however, yet much more highly resolved during both cruise periods.

Table 2. Regression coefficients and statistics for HPLC Chl-a and *in situ* $a_{LH}(676)$ power function relationships for the cruises PS93.2 and PS99.2. The uncertainties of the regression coefficients A and B were calculated with 95% confidence bounds.

Cruise	Measuring method	A	B	R^2	RMSE	MAE	N
PS93.2	AC-S	86.1 ± 11.1	1.00 ± 0.03	0.90	0.079	0.051	134
	Cary	62.8 ± 9.85	1.05 ± 0.04	0.82	0.114	0.070	134
PS99.2	AC-S	36.2 ± 6.78	0.93 ± 0.05	0.90	0.120	0.083	84
	QFT-ICAM	57.5 ± 10.2	0.91 ± 0.04	0.90	0.133	0.089	104

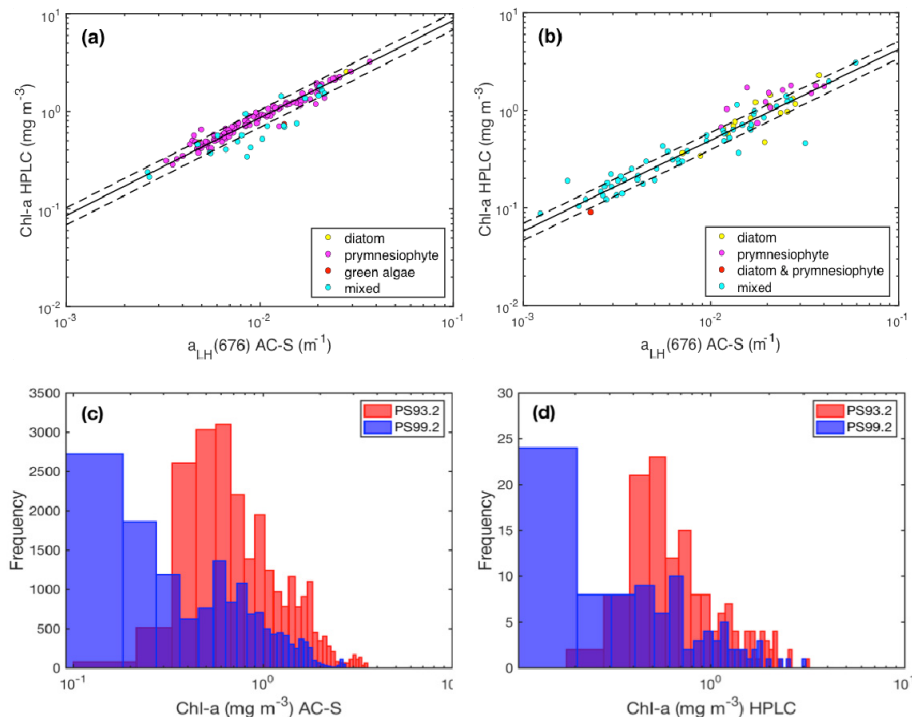


Fig. 2. (a) and (b) show the relationships between the collocated $a_{LH}(676)$ derived from the underway spectrophotometry and HPLC Chl-a data for PS93.2 and PS99.2, respectively. The solid lines are power fits according to Table 2. The dash lines are $\pm 20\%$ error lines. Different colors filled in the circles represent the dominating phytoplankton groups by diatom, prymnesiophyte, both diatom and prymnesiophyte or green algae, while the term “mixed” denotes a mixture of phytoplankton groups with no dominating group; (c) and (d) show frequency distribution of AC-S derived and HPLC Chl-a.

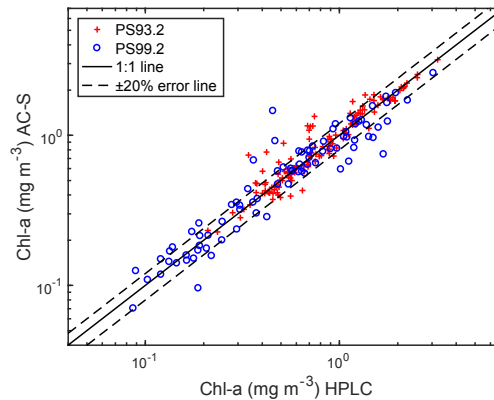


Fig. 3. Comparison between Chl-a data obtained from underway spectrophotometry and HPLC measurements.

The differences in the HPLC Chl-a to AC-S $a_{LH}(676)$ relationships as well as the scatter around the regression lines between the two cruises suggested an inter- and intra-cruise variability of chlorophyll-specific absorption line height. The relationship for PS99.2 exhibited larger variations than that for PS93.2 as inferred from greater *RMSE* and *MAE* values. This may originate from the different times of the years being sampled that favor different phytoplankton growth conditions: PS93.2 was conducted from late July to mid August and had a larger range and higher mean value of Chl-a data (see above); PS99.2 was conducted from late June to mid-July and also contained more very low Chl-a values (Fig. 2(c) and 2(d)). In addition, there were clear shifts of dominating phytoplankton groups (defined here as the fraction of a certain group calculated using DPA greater than 45%): Prymnesiophytes were dominant in 82.8% of the surface waters of PS93.2, while only 1.5% are diatom-dominated and 14.9% of the water samples were mixed without apparent dominating phytoplankton groups. In contrast, the fractions changed to 6.0%, 16.7% and 76.2% for PS99.2, respectively. Figure 2(b) shows that the data points outside of the $\pm 20\%$ error lines can be diatom-, prymnesiophytes-dominated or phytoplankton-mixed samples. Further calculation showed that 73.1% of the “mixed” samples have a proportion of diatoms over 30%. According to Nöthig et al. [29], in the Fram Strait in summertime, prevailing diatoms are *Thalassiosira* spp and *Chaetoceros* spp, mainly *C. socialis*, *Fragilariopsis oceanica* and other pennate diatoms, whereas the main species of prymnesiophytes is in most cases *Phaeocystis pouchetii*. Therefore, we suspected that the more diverse phytoplankton composition observed in PS99.2 samples involved greater variations in cell size and pigment composition and hence, pigment packaging, contributing to the relatively larger discrepancy in the relationship of HPLC Chl-a data and AC-S derived $a_{LH}(676)$. Additional variability of these relationships is expected due to the absorption in the line height region by non-algal particles and CDOM [68], and to the assumption that CDOM absorption during non-filtering period of the underway AC-S flow-through system linearly varied in the AC-S data correction scheme. The amount of non-algal particles and CDOM may vary strongly between the period of phytoplankton bloom development and degradation.

3.2 Satellite Chl-a validation

The reconstructed *in situ* Chl-a data sets from the AC-S flow-through system along the cruise tracks were directly compared with the spatial and temporal coincident satellite Chl-a products. *In situ* Chl-a data were used to validate Chl-a operational products retrieved from MODIS-A OCI operational algorithm for PS93.2 and from MODIS-A OCI, OLCI OC4 and C2RCC operational algorithms for PS99.2. Furthermore, Polymer-Standard, OCI- and OC4-Polymer algorithms were compared and assessed. In addition, validation of the same Chl-a products and assessment of the above algorithms using HPLC Chl-a were also performed for

comparison. Summary statistics are presented in Table 3. The r , $RMSE$, δ and Δ were calculated in log10 space, while RPD was calculated in linear space. Figure 5 shows the density plots of the validation results.

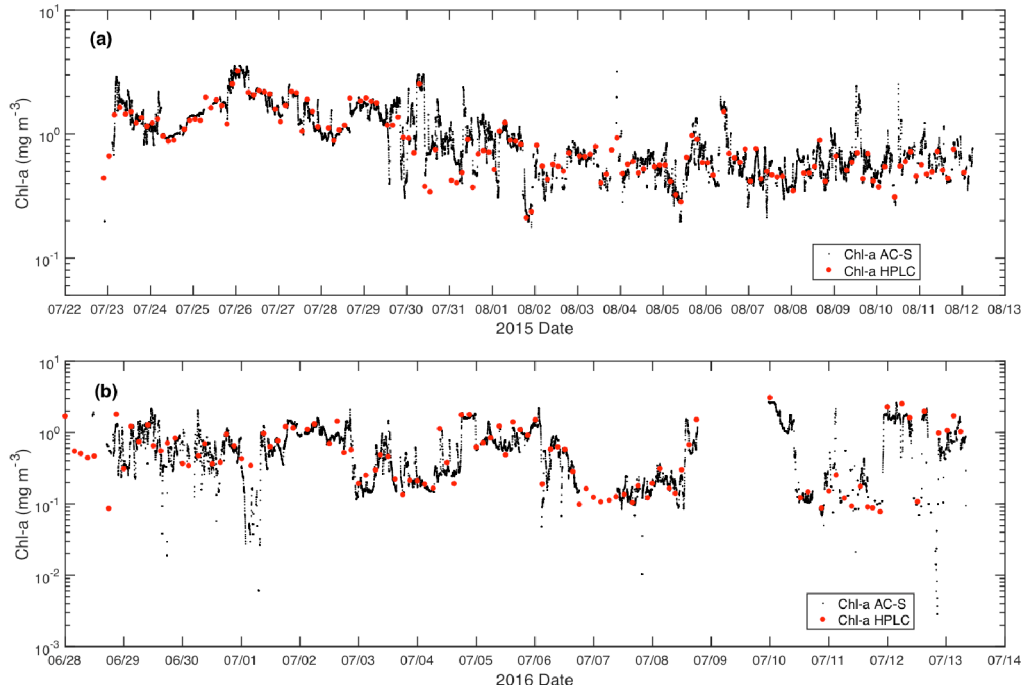


Fig. 4. Time series of AC-S derived and HPLC Chl-a data during the cruise period of (a) PS93.2, and (b) PS99.2.

As is shown in Table 3, the number of match-ups generated by AC-S derived to satellite Chl-a (hereinafter denoted as “AC-S matchups”) is over one order of magnitude greater than those from HPLC to satellite Chl-a (hereinafter denoted as “HPLC matchups”). For PS93.2, the number of AC-S matchups for MODIS-A is 80, in contrast with only 8 HPLC matchups. For PS99.2, the numbers of AC-S matchups from the three Polymer atmospheric correction method based algorithms (i.e. OLCI Polymer-Standard, OCI- and OC4- Polymer algorithms) and OLCI C2RCC algorithm are two to three times greater than those by the operational MODIS-A OCI and OLCI OC4 algorithms. This is because OLCI C2RCC and Polymer are the atmospheric correction processors that incorporate the contributions of sun glint and thin clouds in their reflectance models to derive atmospheric corrected remote sensing reflectance, allowing for much larger coverage of data [72,73]. MERIS Polymer products have shown to improve the spatial coverage by almost a factor of two [74] and have proven successful for retrieving (MERIS) ocean color products: Polymer was selected as the MERIS processor for atmospheric correction for the Ocean Color Climate Change Initiative (OC-CCI) after an extensive validation and intercomparison with other atmospheric correction algorithms in which each algorithm’s uncertainty was assessed [73].

When considering the correlation between *in situ* and satellite data sets, for PS99.2, both AC-S derived and HPLC Chl-a data were reasonably correlated with the corresponding satellite Chl-a retrieved from the operational band ratio algorithms (i.e. OLCI OC4-Operational and MODIS-A OCI) ($r > 0.87$ and 0.79 , respectively) and the three Polymer based algorithms ($r > 0.94$ and 0.96 , respectively). However, the correlation coefficient significantly decreased when comparing Chl-a data from MODIS-A OCI algorithm to AC-S Chl-a for PS93.2 ($r = 0.25$). The decrease is even more significant for OLCI C2RCC algorithm ($r = 0.13$). Furthermore, the regression slopes for C2RCC algorithm ($S = 0.07$ and

0.11 with respect to AC-S and HPLC measurements, respectively) are far from the unity. A reason could be that those satellite Chl-a have less dynamic range than other satellite Chl-a products (Fig. 5(g) and 5(h)). Nevertheless, the density plots of OLCI C2RCC match-up analysis showed that a considerable proportion of match-up points were around the one-to-one line (Fig. 5(g) and 5(h)). For PS93.2, the regression slopes for MODIS-A OCI Chl-a to both AC-S and HPLC based data sets are 1.04 and 1.14, respectively. For PS99.2, except for OLCI C2RCC and OC4-Operational products, the slopes for all the other satellite algorithms for both AC-S and HPLC match-ups are close to or greater than the unity. For example, the slope for OLCI Polymer-Standard to HPLC Chl-a is 0.90 and to AC-S derived Chl-a 1.61, whereas for OC4-Operational they are 0.60 and 0.75, respectively.

Table 3. Summary statistics of linear regression analysis between *in situ* and coincident satellite Chl-a data.

Cruise	Satellite Sensor	Algorithm	<i>In situ</i>	<i>N</i>	<i>S</i>	<i>I</i>	<i>r</i>	<i>RMSE</i>	δ	Δ	<i>RPD</i> (%)
PS93.2	MODIS-A	OCI	AC-S	80	1.04	-0.08	0.25	0.302	-0.056	0.297	13
		OCI	HPLC	8	1.14	-0.41	0.92	0.380	-0.258	0.280	-34
PS99.2	MODIS-A	OCI	AC-S	512	3.33	-0.23	0.95	0.473	0.445	0.160	199
		OCI	HPLC	91	2.60	-0.09	0.79	0.449	0.402	0.200	47
	OLCI	Polymer-Standard	AC-S	2706	1.61	0.11	0.94	0.392	0.332	0.207	137
		Polymer-Standard	HPLC	257	0.90	0.16	0.96	0.229	0.118	0.196	43
		OCI-Polymer	AC-S	2077	1.98	-0.02	0.95	0.395	0.345	0.192	140
		OCI-Polymer	HPLC	213	1.12	-0.03	0.98	0.143	-0.061	0.129	19
		OC4-Polymer	AC-S	3396	3.38	-0.65	0.95	0.461	0.430	0.166	185
		OC4-Polymer	HPLC	212	1.71	-0.25	0.98	0.196	0.123	0.152	39
		OC4-Operational	AC-S	789	0.60	0.29	0.87	0.395	0.274	0.284	125
		OC4-Operational	HPLC	97	0.75	0.27	0.97	0.474	0.381	0.282	186
C2RCC	AC-S	2144	0.07	0.16	0.13	0.282	0.048	0.278	34		
C2RCC	HPLC	271	0.11	0.13	0.47	0.230	-0.092	0.211	-10		

Considering all four uncertainty measures of *RMSE*, Δ , δ and *RPD* with respect to the *in situ* AC-S measurements, OLCI Polymer-Standard algorithm yielded the most reliable estimation of Chl-a, closely followed by OCI-Polymer algorithm. Both OLCI Polymer-Standard and OCI-Polymer algorithms showed small values of Δ (0.207 and 0.192, respectively), which indicates a good estimating precision. Moreover, the bias quantified in terms of δ (0.332 and 0.345, respectively) and *RPD* (137% and 140%, respectively) are relatively small, ensuring the reasonable accuracy for these two algorithms. OLCI OC4-Polymer and MODIS-A OCI (PS99.2) algorithms performed similarly, providing the smallest values of Δ (0.166 and 0.160, respectively), and yet, higher uncertainty in terms of δ , *RPD* and *RMSE*. OC4-Operational algorithm performed better than OLCI OC4-Polymer and MODIS-A OCI (PS99.2) algorithms in terms of the smaller *RMSE*, δ , and *RPD*, and yet, a large Δ . OLCI C2RCC and MODIS-A OCI (PS93.2) showed much smaller δ (0.048 and -0.056, respectively) and *RPD* (34% and 13%, respectively) than other algorithms. However, the data dispersion indicated by Δ is much higher for these two algorithms, inferring a less precise estimation of Chl-a. The lower bias measures are probably because that the positive and negative errors cancelled each other, as shown in Fig. 5(b), and 5(h), whereas all the other algorithms mostly provided positive errors.

Overall, the Polymer-Standard and OCI-Polymer products gave the most reliable results among the six considered satellite products. The good performances of OCI-Polymer and Polymer-Standard algorithms may be attributed to the successful atmospheric correction of adjacent effects due to snow/ice and clouds in the study area [48,49]. However, when compared to AC-S data, their overestimation indicated by RPD was one order of magnitude higher than MODIS-A OCI for PS93.2. For PS99.2, MODIS-A OCI showed similar high values of uncertainty as OLCI OC4-Polymer products. The OCI and OC4 algorithms are both empirical algorithms that use a three-band and a four-band blue-green reflectance ratio, respectively, to directly retrieve Chl-a. These data products performed well when evaluated using a global data set, probably due to their immunity to scale errors or instrument noise in remote sensing reflectance data [65]. The OLCI C2RCC products showed relatively low uncertainty and low bias (small negative/positive bias for HPLC/AC-S match-ups), but had yet the least correlation to the *in situ* data sets among all operational products. Though C2RCC is used to generate the Case 2 water products of Sentinel-3 OLCI standard ESA products, it is based on an artificial neural network trained for a wide range of atmospheric and ocean optical conditions [75,76]. Moreover, its Chl-a products are estimated using particulate absorption at 440 nm derived from remote sensing reflectance [75,76], making the C2RCC algorithm work reasonably well in our study area.

MODIS-A OCI Chl-a products had relatively low uncertainty for PS93.2 and tended to underestimate Chl-a data at relatively low Chl-a values indicated by the negative value of δ . It may be attributed to the dominance of prymnesiophytes in the surface waters of PS93.2 (Fig. 2(a)). *Phaeocystis pouchetii*, the most likely main species of prymnesiophytes in our study area (mentioned in 3.1.) [29], is able to form large colonies that have strong self-shading, lowering the specific absorption coefficient and causing the underestimation of satellite Chl-a retrievals. However, overall, MODIS-A OCI (PS93.2) overestimated Chl-a, especially at relatively high Chl-a values (Fig. 5(b)). As pointed out above for PS99.2, MODIS-A OCI and OLCI OC4-Operational and three Polymer based products were characterized by an overestimation, as positive δ and RPD displayed. However, there is a proportion of underestimated Chl-a from OLCI C2RCC products when compared to HPLC data ($RPD = -10\%$) and overestimation ($RPD = 34\%$) when compared to AC-S data. For PS99.2, the Chl-a overestimation was significant for OLCI OC4-Polymer and MODIS-A OCI ($RPD \geq 185\%$) and slightly less significant for OLCI Polymer-Standard, OCI-Polymer and OC4-Operational ($100\% \leq RPD \leq 140\%$). The overestimation of Chl-a by band ratio algorithms is consistent with previous match-up analysis that Chl-a is overestimated by OC4 algorithm in the Arctic Ocean [14,77]. This is because CDOM concentrations in the Arctic Ocean are much higher than the global average, challenging the global empirical relationships underlying OCI and OC4 algorithms. It also explains the overestimation by the Polymer standard Chl-a product which is retrieved assuming a variability of the ocean model depending only on two parameters, the Chl-a and a backscattering coefficient, not accounting for additional CDOM variability [48,49], which implies a (global) constant relationship between phytoplankton and other absorbing water constituents, i.e. CDOM and non-algal particles. As a consequence, an excess of CDOM can be interpreted as an additional concentration of Chl-a.

For a given satellite algorithm, AC-S and HPLC match-ups have different uncertainty measures and regression parameters for both cruises. This is especially true for MODIS-A OCI Chl-a products for PS93.2 and OLCI C2RCC Chl-a products for PS99.2, where different trends (i.e. overestimation or underestimation) of satellite Chl-a estimates were observed. This might be because of the insufficient coverage of HPLC data points. The density plots (Fig. 5) show that spatial and temporal variability of satellite data is accounted for to a greater extent when doing match-up analysis against AC-S data set.

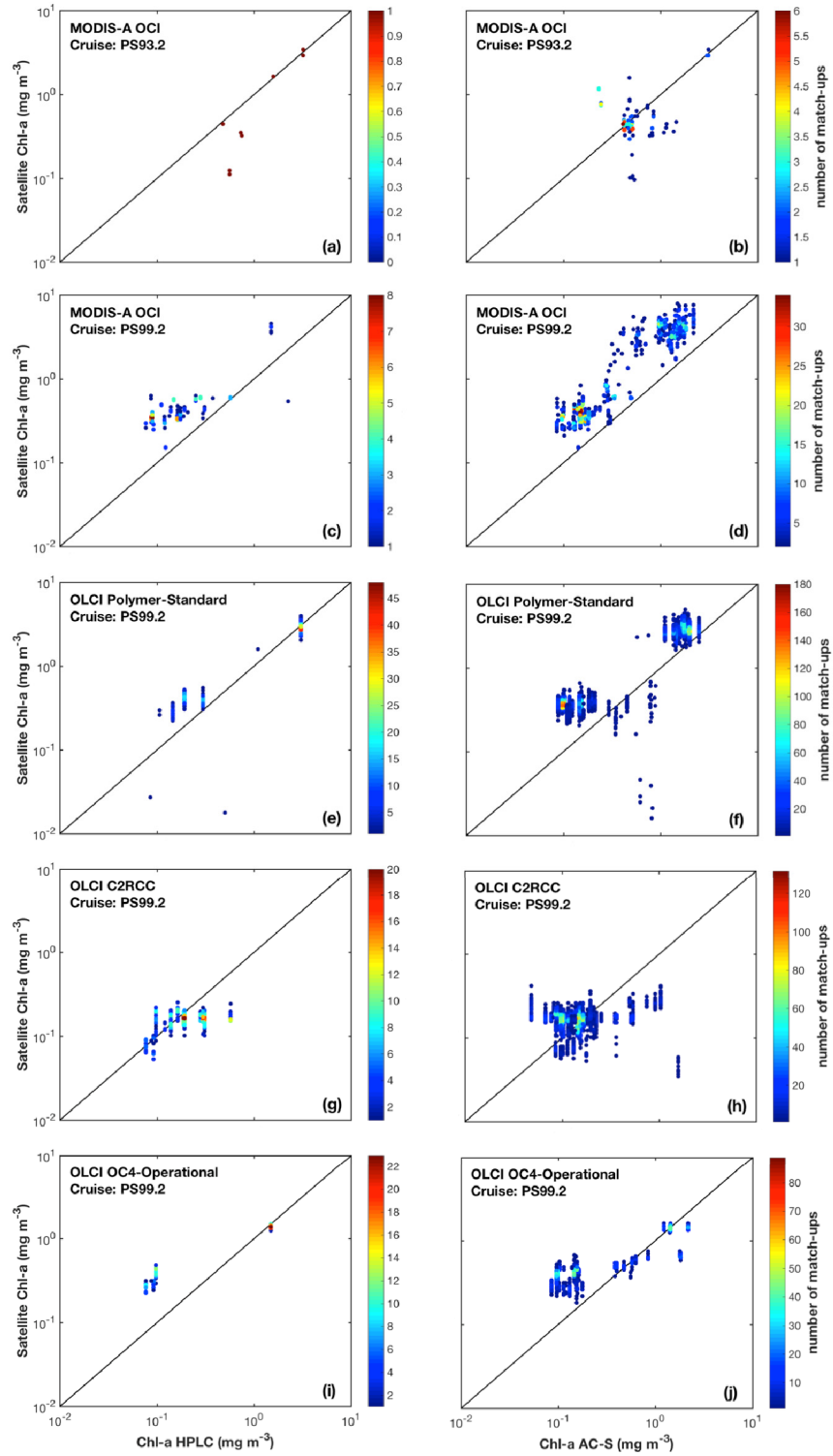


Fig. 5. Density plots of satellite to *in situ* match-up analysis.

In summary, validation results revealed acceptable performances of the operational band ratio algorithms (OCI, OC4) that are applied to the MODIS-A and OLCI sensors. Better results were achieved with the Polymer atmospheric correction algorithm applied to OLCI data. Overall, all the algorithms tended to overestimate Chl-a in the Fram Strait to various extent. The OLCI Polymer standard output provided the most reliable Chl-a estimates, and nearly as good results were obtained from the OCI-Polymer algorithm. The OC4-Operational algorithm performed slightly better than OC4-Polymer algorithm. The OLCI C2RCC Chl-a products showed relatively low uncertainty, but had yet the least correlation to the *in situ* data sets. MODIS-A OCI Chl-a products during the cruise period of PS93.2 did not correlate well to AC-S derived *in situ* AC-S derived Chl-a, but had yet relatively low uncertainty. For PS99.2, they showed similar high values of uncertainty as OLCI OC4-Polymer products. Further assessment of other types of Chl-a algorithms, e.g. semi-analytical methods (e.g., Quasi-analytical-algorithm (QAA) from Lee et al. [78] or Garver-Siegel-Maritorena (GSM) from Maritorena et al. [79]) or selection of neural network approaches based on water types [80] are necessary to be exploited to obtain optimized Chl-a data sets for the Fram Strait. Especially when Polymer atmospheric correction method is applied, high data coverage with low uncertainty can be expected.

4. Conclusion

We have shown the applicability of using the underway AC-S flow-through technique to continuously measure particulate absorption at high frequency in the Fram Strait. For the first time in this region, the relationships between AC-S derived particulate absorption and HPLC Chl-a were assessed during two summer cruises (PS93.2 in 2015 and PS99.2 in 2016). The good power law correlation enabled the estimation of continuous surface Chl-a along the entire cruise tracks. The continuous *in situ* data sets obtained from the underway AC-S flow-through system were used to validate satellite operational Chl-a products from MODIS-A OCI and OLCI OC4-Operational, C2RCC and Polymer-Standard algorithms, and to assess the performances of Polymer-Standard, OCI- and OC4-Polymer algorithms. For comparison, the validation of satellite operational products and assessment of different algorithms were also performed using HPLC measurements.

Statistics of linear regression analysis between *in situ* measurements and co-located satellite data for both cruises in the Fram Strait indicated reasonable performances of all algorithms. When considering AC-S match-ups, all algorithms were characterized by an overestimation of satellite Chl-a. However, there is underestimation of Chl-a for MODIS-A OCI (PS93.2) and OLCI C2RCC. This underestimation is also determined for HPLC match-ups. The OLCI Polymer-Standard and OCI-Polymer products had relatively high estimation precision and small bias with respect to both *in situ* AC-S and HPLC data sets, suggesting a successful atmospheric correction and the most reliable approximations of Chl-a data by OLCI Polymer-Standard and OCI-Polymer algorithm in the Fram Strait. When using HPLC data, the numbers of collocations are much lower, highlighting the capability of underway spectrophotometry to generate more sufficient surface Chl-a data sets for satellite Chl-a products validation and algorithms assessment in the Fram Strait. With the help of further automatic acquisition of AC-S data, the establishment of a long-term data record of satellite Chl-a data with determined uncertainties for this under-sampled remote area to be used in climate change research will be expected.

Funding

FRontiers in Arctic marine Monitoring (FRAM) project of Helmholtz Association Infrastructure Programme; Transregional Collaborative Research Center (TR 172) “Arctic Amplification: Climate Relevant Atmospheric and SurfaCe Processes, and Feedback Mechanisms (AC)3” via the subproject C03, funded by the German Research Foundation

(DFG, Deutsche Forschungsgemeinschaft); China Scholarship Council (CSC); POLMAR Helmholtz Graduate School for Polar and Marine Research of the Alfred-Wegener-Institute.

Acknowledgments

We thank all the scientists, especially the chief scientist Thomas Soltwedel, the captains and crew on *R.V. Polarstern* for their support for collecting the *in situ* data used in this paper during the cruises PS93.2 and PS99.2. We acknowledge the discussions with Emmanuel Boss, Nils Haëntjens, Svetlana Loza and Hongyan Xi on AC-S data analysis and the interpretation of satellite validation. We thank Yashen Wang, Yanqun Pan, Jan Streffing, Xun Gong and Yuchen Sun for their suggestions in improving the codes for data processing. We thank Maryia Herasimava for helping quality control the HPLC data. We also thank Haozhuang Wang, Heng Wang, Saeid Bagheri Dastgerdi and Jan Streffing for their comments on English writing. We would also like to thank the Ocean Biology Processing Group of NASA for the processing and distribution of MODIS-A data and ESA/EUMETSAT for providing Sentinel-3 OLCI data used in the paper. We are grateful to the anonymous reviewers whose comments significantly improved the manuscript. All *in situ* data of our study are available at <https://doi.org/10.1594/PANGAEA.885631>.